Photocatalytic degradation of Remazol Red B and Rhodamine B dyes using TiO$_2$ nanomaterial: estimation of the effective operating parameters

Farid I. El-Dossoki[a], Tarek M. Atwee[b], Ahmed M. Hamada[a], Ashraf A. El-Bindary[c],*

[a]*Chemistry Department, Faculty of Science, Port-Said University, Port-Said 42526, Egypt*
[b]*Physics Department, Faculty of Science, Damietta University, Damietta 34517, Egypt*
[c]*Chemistry Department, Faculty of Science, Damietta University, Damietta 34517, Egypt, email: abindary@yahoo.com*

ABSTRACT

The presence of persistent organic pollutants (POPs) including dyes in the aquatic ecosystem is of major concern worldwide because of their hazardous effect, and human and environmental risks. The degradation of conventional wastewater plants costs a lot, due to increased environmental restrictions. Using photocatalysis to remove (POPs) is a promising, effective and sustainable process. A simple one-step sol–gel procedure for degradation of Remazol Red B (RRB) and Rhodamine B (RhB) has been used to synthesize titanium dioxide photocatalyst. Various techniques, such as X-ray diffraction, scanning electron microscopy, energy-dispersive X-ray spectroscopy, Brunauer–Emmett–Teller, and parameters that influence the photodegradation process, including catalyst dose, pH, initial dye concentration, were used to study TiO$_2$ photoactivity. The degradation of TiO$_2$ via UV radiation for RRB and RhB after 75 min was 99.7% and 99.8% respectively. The photodegradation rates for two dyes using a Langmuir–Hinshelwood are shown pseudo-first-order. Besides, reactive species scavengers have been studied during degradation and the major species is OH$^\bullet$ radicals. Photoluminescence experiments using terephthalic acid as a reference molecule determined OH$^\bullet$ free radical formation during irradiation.

Keywords: TiO$_2$; Catalytic degradation; Sol–gel; Rhodamine B; Remazol Red B; Kinetics

1. Introduction and background

Environmental sustainability needs two major requirements: reduced waste production and treatment of waste materials once it is formed. Dyes are an important class of aquatic pollutants: About 700,000 tons of world-wide organic dyes are annually produced [1,2], between 10%–15% of dyes are lost in effluents during dyeing and application processes [3]. These dye-polluted effluents contain non-biodegradable, carcinogenic, highly hazardous, and colored pigments that make wastewater toxic and high in both chemical oxygen demand and biochemical oxygen demand [4–6].

These dyes are shown resistance to biological further than physical and chemical treatment strategies and limited effect. Conventional biological treatment methods do not achieve significant dye decolorization and degradation because of their high aromatic content and dyes molecules' stability [7,8]. Under anaerobic biodegradation conditions, the azo bond transformed into aromatic amines which are carcinogenic, not metabolized anaerobically, and more dangerous than dyes [9–11]. Physical methods, such as adsorption, is non-destructive since it just transfers dyes from a liquid phase into a solid phase. Thus, causing secondary hazardous pollution [12,13]. Coagulation, using alums,

* Corresponding author.

ferric salts, or limes, is also a low-cost process. However, it requires the disposal of waste [10]. Chemical techniques (ozonation, chlorination) usually help to destroy the structures of chromophoric dyes. But mineralization is still not complete. Decolorization is caused by chemical reactions through ozonation and chlorination. Chlorinated organics can be more toxic than the dye itself, which is a by-product of chlorination [14,15].

Filtration potentially such as flocculation, reverse osmosis, and adsorption on activated carbon has also been tested and provides pure water but low-molar-mass dyes can pass through the filter system [10,11,13]. As in very low concentrations (under 1 ppm), dyes are still clearly visible in water and have a considerable influence on the water environment [16,17].

However, all these techniques are useful and versatile, but they all end up producing a secondary waste product requiring cost-effective treatment to complete dye's mineralization.

Among the alternative oxidation methods called advanced oxidation processes (AOP), heterogeneous photocatalysis has appeared as an emerging destructive technology leading to the total mineralization of most organic pollutants [18]. AOPs are considered clean technologies to treat polluted waters that apply the concept of producing hydroxyl radicals (OH⁻) that attack the organic pollutants [19]. The efficiency of AOPs is based on the generation of these highly reactive radicals that are unselective and powerful oxidizing species (E^o = 2.80 V) which involves the complete photo-mineralization or oxidation of the target contaminants into CO_2, H_2O, and inorganic ions with a higher biodegradability and/or lower toxicity of the reaction byproducts [20,21]. AOPs can be applied as post-treatment or pre-treatment of biological processes. Titanium dioxide (TiO_2), has a significant degradation effect as a good photocatalyst of aquatic dye pollutants because of its chemical stability, nontoxic nature, low cost, handiness, hydrophobicity, protection for antimicrobial activity, flammable retardation, and highly reactive nature under UV irradiation, as well as produce self-cleaning materials [22] crystal structure, particle size, specific surface area, and porosity affect TiO_2 photocatalytic activity [23]. For this study, Remazol Red B and Rhodamine B dyes were chosen. Rhodamine B is a well-known fluorescent water tracer that is used in textile industries and foodstuffs which irritate human beings and animals' eyes, skin, and respiratory tract [24]. Remazol Red B is a vinyl sulphone-reactive dye used in textiles, which is mutagenic and hard to be degraded by aquatic living organisms [25].

In the present research study, TiO_2 nanoparticles were prepared via a sol–gel process at 550°C calcination temperatures. Different techniques described the crystal structure and the chemical characteristics of the catalyst. The process conditions, including catalyst dosage, pH, initial concentration dyes, were optimized for the photo-degradation process. Different concentrations of dye have been tested with optimized degradation efficiency, and it is the highest for Rhodamine B (RhB) and Remazol Red B (RRB) dyes at 6–25 mg L⁻¹, respectively. There is also a generalized mechanism for RhB and RRB dye chemical reactions during photocatalysis.

2. Materials and methods

2.1. Raw materials and reagents

2.1.1. Raw materials and reagents

Titanium tetra isopropoxide (TTIP) ($C_{12}H_{28}O_4Ti$) and dodecylamine ($C_{12}H_{27}N$) were purchased from Sigma-Aldrich (United States) chemicals and used as received. Rhodamine B and Remazol Red B as a textile industry pollutant model were supplied by Sigma-Aldrich (United States) chemicals and were used as received (Table 1). A stock solution of dyes whose concentration was 1.0 g L⁻¹ was used and could be diluted to the required concentration with deionized water in the experiment. All chemical reagents were of analytical grade and used with no further purification. The samples were then preserved in the desiccator for further use over anhydrous $CaCl_2$.

2.2. Synthesis of TiO_2 photocatalyst

There are several methods for preparing TiO_2 nanoparticles, including the technique of mechanochemical use, a soft chemical method, the method of wet chemical use, the method of micro-emulsion and the method of sol–gel, in which the route to sol–gel is cheaper and simplified and, an effective way of synthesizing nanoparticles. The addition of a surfactant or capping agent to this method is a common practice for reducing the particle size, preventing and generating highly monodisperse nanoparticles [26]. By using the dodecylamine as a structural directing agent, a single-step sol–gel process synthesized a mesoporous TiO_2 nanocrystal. In particular, 1 g of dodecylamine was dissolved in 10 mL of water and 90 mL acetonitrile and then added dropwise to 8 mL of TTIP dissolved in 20 mL ethanol. Then the mixture was aged continuously stirred for 24 h at room temperature. The precipitate was filtered, then dried for 6 h at 100°C. To get the TiO_2 mesostructured and remove the surfactant, the calcination of the obtained mesostructured hybrids in the air for 8 h was 550°C with a heating rate of 1°C/min and a cooling rate of 2°C/min.

2.3. Morphological and optical characterization

The bond vibration of TiO_2 powder was analyzed by Fourier-transform infrared spectroscopy (FT-IR) analysis and carried out using a JASCO-FT/IR-4100 spectrometer (JASCO, Easton, MD, USA): the finely ground sample of TiO_2 was included into KBr discs before analysis in the wavenumber range 500–4,000 cm⁻¹. The surface morphology and particle size of the TiO_2 photocatalyst were examined using a scanning electron microscopy (SEM) analysis at accelerating voltages of 20 kV (JEOL JSM-6510LV, USA). The elemental distribution of TiO_2 was analyzed using the energy-dispersive X-ray spectroscopy (EDX) and taken on a Leo1430vp microscope with an operating voltage of 5 kV. Structural variations of the as-prepared materials were investigated by X-ray diffraction (XRD) technique using a Shimadzu XRD-6000 diffractometer (Shimadzu Corporation, Tokyo, Japan) equipped with Cu Kα radiation (λ = 1.54 Å). The 2θ range was varied

Table 1
Properties of Rhodamine B (RhB) and Remazol Red B (RRB) dyes

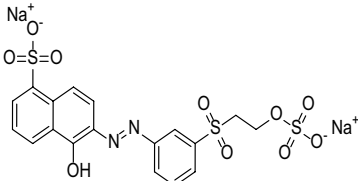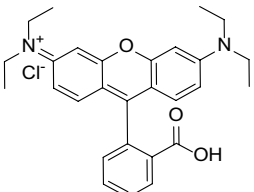| Anionic dyes	Abbr.	M_W	λ_{max}	Chemical formula	Chemical structure
Remazol Red B	RRB	562.52	517	$C_{19}H_{18}N_2O_{11}S_3 \cdot 2Na$	
Rhodamine B	RhB	479.02	553	$C_{28}H_{31}ClN_2O_3$	

Table 2
Crystallographic parameters of TiO_2 calculated from the XRD pattern are listed below

d-spacing (d)	3.4684 Å
Lattice parameter (a)	4.905 Å
Volume (V)	135.372 Å^3
Density (ρ)	4.068 g cm^{-3}
Crystallite size (D)	13.1 nm
Micro strain (ε)	2.6709×10^{-3} L^{-2} m^{-4}
Specific surface area (S_a)	112.589×10^6 cm^2 g^{-1}

between 5°–80° at a scanning rate of 0.02°. The crystal system, space group, and lattice parameters values were considered and optimized using CRYSFIRE and CHEKCELL computer programs [27]. UV-Visible spectrophotometer (PerkinElmer AA800 spectrophotometer Model AAS, China) was employed for absorbance measurements of samples using a 1.0 cm quartz cell. A fluorescence spectrometer (Thermo Scientific Lumina, UK) was used for fluorescence measurements of samples using a 1.0 cm quartz cell. The adsorption/desorption isotherm of N_2 on TiO_2 at 77 K was performed with a Quantachrome Touch Win Instruments Version 1.11. For the analysis of the curves, we utilized the Brunauer–Emmett–Teller (BET) method (p/p_o from 0.05 to 0.35) for a specific area, the t-plot method for the external area, volume, and area of micropores; and the Barrett–Joyner–Halenda (BJH) method for diameter determination of mesopores. The zeta potential of the TiO_2 was measured using a Nano Zetasizer (Nano ZS Malvern Instruments Ltd., London, United Kingdom) at various pHs from 2 to 12. A 0.01 g of the TiO_2 was mixed with 50 mL of 0.1 M KCl. The suspension was then adjusted to the specified pH and kept under stirring for 15 min. After conditioning, the suspension was left for another 15 min for settling before measurements, Hanna Instruments pH meter (model 211) was used for pH adjustment.

2.4. Photocatalytic activity of prepared TiO_2 in the degradation of RRB and RhB solutions

A photocatalytic process of the TiO_2 photocatalyst was applied with an ultraviolet lamp to monitor the photodegradation of Remazol Red B (RRB) and Rhodamine B (RhB) under atmospheric conditions in an aqueous solution. In the experiment the UV-lamp specified by λ_{max} (nm) 280–100 with E_{photon} (eV) 4.43–12.4 is used [28]. The reactor used to carry out dye degradation experiments was one 150 mL beaker (5 cm in diameter the distance between the lamp and the top surface solution was fixed at 10 cm the reactor work volume was 100 mL, which involved a dye solution and the suspension of a photocatalyst. TiO_2 (2.5 g L^{-1}) samples were applied to 100 mL RhB (6 mg L^{-1}) and RRB (25 mg L^{-1}) dye to achieve even dispersion of the photocatalyst, the efficient agitation of the dye solution and the photocatalyst is needed. The solution has been constantly stirred for 30 min in dark at 800 rpm by a magnetic stirrer to adsorb the dye in the solution for the powder photocatalyst before illumination and reach adsorption–desorption equilibrium.

Therefore, the influence of the surface adsorption is thus eliminated in the removal of RRB and RhB in pHs 2–10 adjusted by HCl (0.1 mol L^{-1}) and NaOH (0.1 mol L^{-1}) the pH effect of the initial solution was measured. The dye concentration of RRB and RRB dye was evaluated with 2.5 g L^{-1} photocatalyst by variation of respective concentrations from 4 to 9 and from 10 to 60 mg L^{-1}. Also, the dosage of catalyst ranged from 0.1 to 0.5 g L^{-1}, in terms of RhB and RRB concentration at 6 and 25 mg L^{-1}, respectively. To remove all suspended solid catalyst particles to analyze them, each sample was removed at a certain time and then centrifuged for 5 min at 20,000 rpm. An exhaust fan is necessary to keep the temperature inside the enclosure. In a spectrophotometer with UV-Visible, the RhB and RRB absorption in the supernatant liquid was recorded at maximum absorption wavelength, RhB ($\lambda_{max} = 554$ nm) and RRB ($\lambda_{max} = 517$ nm).

Eq. (1) determined the rate of degradation (η_D) for the dye:

$$\eta_D\% = \frac{C_0 - C_t}{C_0} \times 100 \tag{1}$$

where C_0 represents the initial absorbance of RhB and RRB solution (blank), and C_t is the absorbance after t minutes of irradiation/reaction. According to Beer–Lambert's law, A_0 and A_t are proportional to C_0 and C_t, where C_0 and C_t are the concentration of blank and sample at (t) time.

According to the Langmuir–Hinshelwood model, photodegradation of pollutants follows the pseudo-first-order kinetics, thus, each dye has a degradation rate studied by Eq. (2):

$$\ln\frac{C_0}{C_t} = k_t \tag{2}$$

The photodegradation rate constant (k, min^{-1}) was calculated from the slope of the straight-line segment of the plot of $\ln(C_0/C_t)$ vs. t as a function of the used experimental parameters.

UV-Visible absorption spectroscopy at room temperature was used to study the optical properties of the photocatalyst. Sonication in paraffin oil dispersed the powder sample and their optical properties were analyzed within the 200–600 nm range using paraffin oil as a reference medium.

3. Results and discussion

3.1. Morphology characterization

3.1.1. BET surface area and pore size analysis

In BET surface area and BJH pore size, TiO$_2$ was investigated with N$_2$ adsorption/desorption methods at 77 K (Fig. 1) [29]. TiO$_2$ nanoparticles N$_2$ adsorption–desorption isotherm is classified as the non-porous solid type II at P/P_o = 0.958. It is completely reversible without a hysteresis loop that illuminates the absence of any pores that allow the capillary process of condensation in isotherm. The specific surface area of TiO$_2$ = 27.418 m^2 g^{-1} calculated by BET equation in its normal range of applicability and adopting a value of 16.2 Å for the cross-section area of the N$_2$ molecule. However, the total pore volume has taken at saturation pressure and expressed as liquid volume = 6.081 × 10^{-2} cm^3 g^{-1}, and the pore distribution of the synthesized material was calculated using the BJH method with an average pore diameter of 8.872 nm [30].

3.1.2. SEM analysis

The surface morphology, size, shape, and growth mechanism of TiO$_2$ nanoparticles at calcination temperature 550°C were evaluated by SEM analysis (Fig. 2). SEM images depicted that these synthesized nanoparticles have agglomeration surface morphology. The agglomeration occurs since the TiO$_2$ nanoparticles have high surface energy, so it is aggregated until it is relatively stable [23]. The SEM result indicates that the TiO$_2$ nanoparticles are formed with an average particles size of about 60 nm. There appears
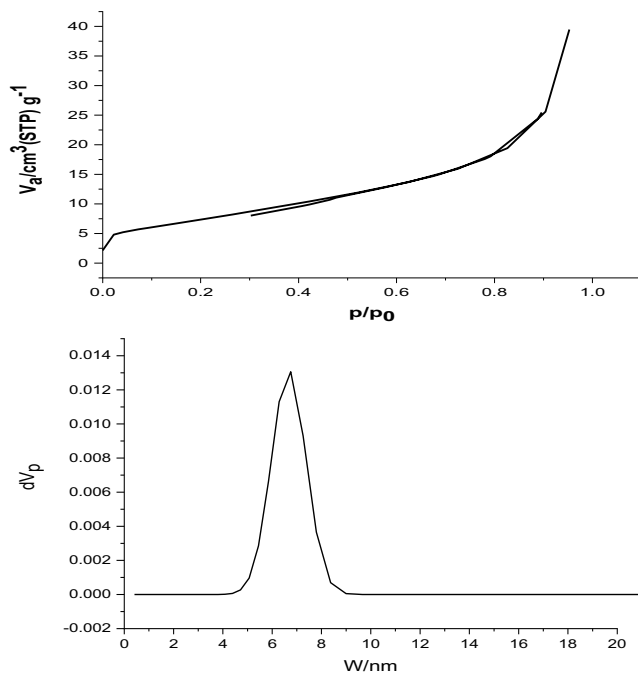

Fig. 1. N$_2$ adsorption/desorption isotherm curve of TiO$_2$ and at 77 K.

some enhancement in the porosity and reduction in the density due to the liberation of gases which created surface pores and holes as obvious from these images [31].

3.1.3. EDX analysis

EDX analysis is based on the principle of unique atomic structure, provides a unique set of peaks on its X-ray spectrum for each element. EDX analysis determined the elementary composition of the TiO$_2$ nanostructure. Ti and O peaks in the spectrum were detected, which provides clear evidence that the synthesized TiO$_2$ is pure and only consists of the Ti and O (Fig. 3). Ti signal at 5.00, 4.50, and 0.40 keV, and oxygen peak at 0.58 keV was observed.

3.2. XRD crystal structure and size of TiO$_2$ catalysts

The XRD patterns of the as arranged TiO$_2$ nanostructures at 550°C are shown in Fig. 4. The observed diffraction peaks communicate to well-crystallized TiO$_2$ indicates the formation of titania and anatase structure (JCPDS No. 21-1272) with a lattice constant $a = b$ = 3.73 Å and c = 9.37 Å [32]. No additional peaks because of impurities were detected indicating the high purity of the as-prepared TiO$_2$, and the peaks at 2θ = 25.66°, 37.31°, 38.11°, 48.45°, 54.27°, 55.35°, 63.00°, 69.02°, 70.30°, 75.51° and 76.1° can be attributed to (101), (004), (112), (200), (105), (211), (204), (116), (220), (215) and (301), planes of TiO$_2$, respectively [33]. The crystallite size (D, Å) of the TiO$_2$ nanoparticles was calculated by using Scherrer's formula [Eq. (3)] [34],

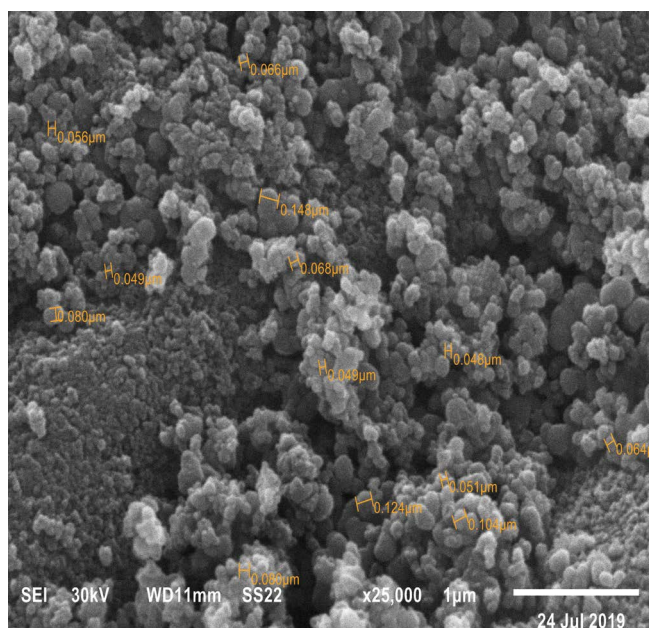$$D = \frac{K\lambda}{\beta\cos\theta_B} \tag{3}$$

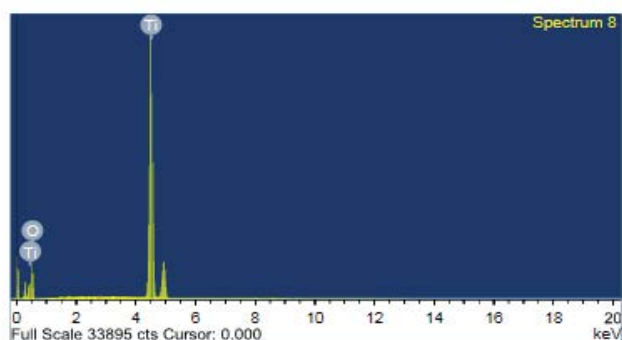Fig. 2. SEM image of TiO_2 nanostructures.

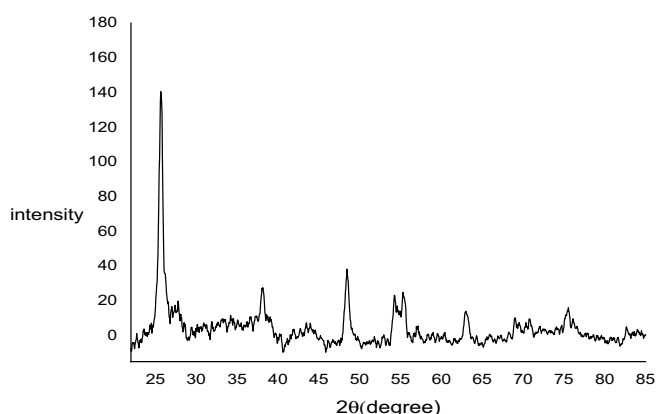Fig. 3. Energy-dispersive X-ray (EDX) spectrum of TiO_2.

Fig. 4. XRD pattern of TiO_2 nanostructures at temperature 550°C.

where λ is the X-ray wavelength (1.54 Å), β is the angular width of the peak at half of its maximum intensity full-width at half-maximum corrected for the instrumental broadening, θ_B is the maximum of the Bragg diffraction peak and K

is Scherrer's constant (0.9 Å). The average crystallite size of TiO_2 was calculated from the main peak ($2\theta = 25.66°$) of XRD patterns, which corresponds to the plane (101). The estimated crystallite size was 13.1 nm. The lattice parameter 'a' was calculated (Table 2) using the relation:

$$d^2 = \frac{a^2}{\left(h^2 + k^2 + l^2\right)} \tag{4}$$

where 'd' is the interplanar distance and h, k and l are the miller indices. The density (ρ) of the samples were calculated from the formula:

$$\rho = \frac{nM}{NV}\left(\text{gm/cm}^3\right) \tag{5}$$

where 'n' represents the number of atoms in the unit cell, 'M' denotes the molecular weight of the sample, 'N' is the Avogadro number and 'V' is the volume of the unit cell. The specific surface area of the samples was calculated using the formula [35]:

$$S_a = \frac{6}{\left(\rho \times D\right)}\left(\text{cm}^2/\text{g}\right) \tag{6}$$

The microstrain of the samples was calculated using the relation [36],

$$\varepsilon = \frac{\beta \cos\theta}{4} \tag{7}$$

3.3. Optical characterization

3.3.1. Optical bandgap energy (E_g)

The quantity of the energy band gap of TiO_2 nanostructures has been determined by studying the optical properties of these particles using UV-visible spectroscopy. The bandgap energy of all nanostructures was calculated depended on the absorption spectrum of the sample according to Eq. (4):

$$E_g = 1,240 / \lambda_g \tag{8}$$

where E_g is the optical band gap energy of the photocatalyst, λ_g is the wavelength in nm used as the absorption edge. Also, the bandgap energy was determined using Tauc's formula [37] which shows the relationship among the absorption coefficient as follows:

$$\left(\alpha h\nu\right)^{1/n} = A\left(h\nu - E_g\right) \tag{9}$$

where α is the absorption coefficient, h is Planck's constant and υ is the frequency ($\upsilon = c/\lambda$, λ is the wavelength, c is the light speed). For the allowed direct bandgap, the value of n equal to 1/2. Exponent n depends on the type of transition and it may have values 1/2, 2, 3/2, and 3

corresponding's to the allowed direct, allowed indirect, forbidden direct, and forbidden indirect transitions, respectively [38]. *A* is a constant and called band tailing parameter. Thus, the bandgap energy was obtained graphically from $(\alpha h\nu)^2$ vs. *hv* for direct transition, extrapolating the linear part on the abscissa according to Eq. (5) (Fig. 5). The bandgap energy was found to be 3.30 eV.

3.3.2. Fourier-transform infrared spectroscopy

The purity and nature of the metal nanoparticles were determined by FT-IR experiments (Fig. 6). In a fingerprint area, metal oxides typically give absorbent bands under 1,000 cm⁻¹, which are caused by inter-atomic vibrations. The vibrations of Ti–O–Ti and Ti–O linkages in the TiO_2 morphology are responsible for the absorption band with respectively 667 and 518 cm⁻¹ [39]. C–H stretching vibrations of the alkane group and symmetric stretching of the carbonyl group is assigned to peaks around 2,925 and 1,437 cm⁻¹. The alkane and carbonyl groups are the results of titanium isopropoxide and ethanol as a precursor material for the synthesis process. The peaks approximately 3,317 and 1,630 cm⁻¹ corresponds to the O–H stretching and bending vibrations of surface-adsorbed water Ti–OH [40].
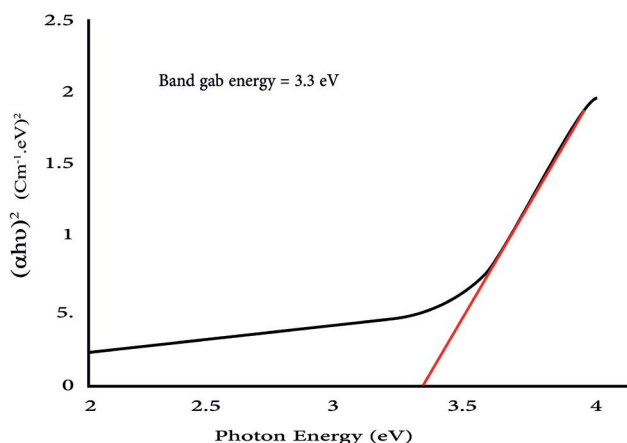

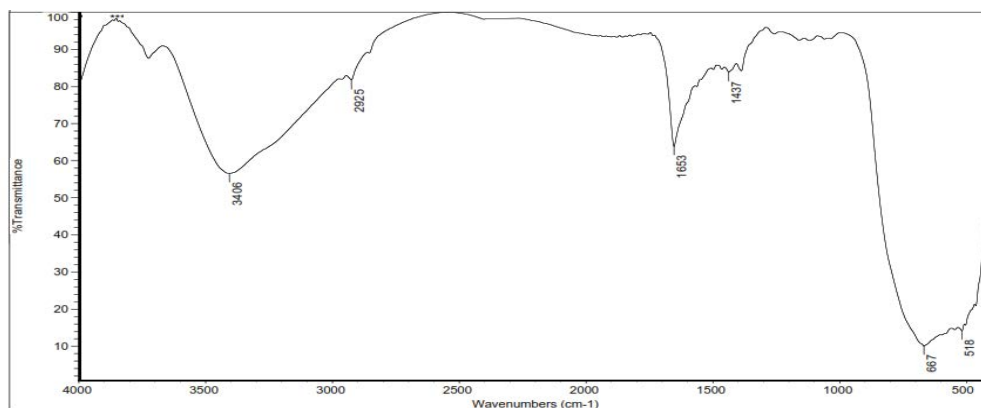Fig. 5. The optical bandgap energy determination of TiO_2 using Tauc's model for *n* = 2.

3.4. Determination of point of zero charge (pH_PZC)

The pH is one of the most significant degradation parameters of RhB and RRB, as it determined the close ionic species in the adsorbate solution and the sorbent surface charge. The pH_{PZC} was calculated by a zeta potentials analyzer of the sample at various pHs. The pH_{PZC} of nanoparticles is a pH value where the zeta potential or net charge is zero on the surface of nanoparticles [41]. The pH_{PZC} value of TiO_2 is approximately 7.2 ± 0.1 (Fig. 7). This demonstrates that the TiO_2 has a positive charge under this pH because of the protonation of the functional groups, and a negatively charged on the TiO_2 surface occurs above this pH. This value depends on the operating conditions such as the measuring instrument, the supporting electrolyte, and the nature of the material.

3.5. Effect of operating parameters on the photocatalytic degradation of RhB and RRB

The photocatalytic degradation of RhB and RRB dye through sol–gel synthesized titanium dioxide TiO_2 revealed the following results.

3.5.1. Effect of initial dye concentration

Both mechanistic and application perspectives important for study the dependence of photocatalytic reaction on the substrate concentration [42]. The initial dye concentration effect on its degradation was investigated with variable dye concentrations of 10–60 mg L⁻¹ in RRB and 4–9 mg L⁻¹ in RhB, with a TiO_2 catalyst concentration of 2.5 g L⁻¹ (Fig. 8) [39]. It is observed that the degradation efficiency of the TiO_2 sample was initially increased for dye concentration up to 6 mg L⁻¹ for RhB and up to 25 mg L⁻¹ for RRB and then decreased. Thus the removal efficiency of dye could be improved by the lower the initial dye concentration [43]. This can be explained because the degradation rate increases with the increase of dye concentration to a certain level and a further increase in dye concentration contribute to a decrease in the degradation rate of the dye [44]. If the initial dye concentrations increase, the probability of reaction between oxidizing species and dye molecules also increases, contributing
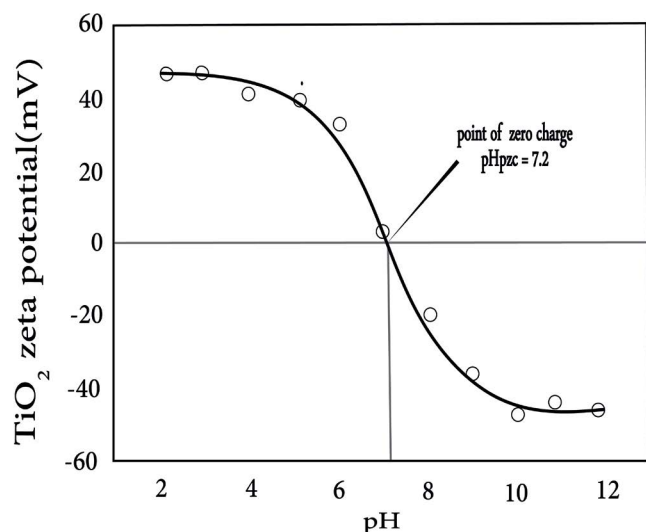

Fig. 6. FT-IR spectrum of sol–gel TiO_2.

Fig. 7. Variation of the zeta potential of TiO_2 as a function of the pH at 550°C.

Fig. 8. Effect of initial dye concentration on the photodegradation activity of TiO_2 at 550°C (20 min of irradiation time 2.5 g L^{-1} TiO_2 and pH = 7).

to an enhancement in the rate of decolorization. The dye degradation efficiency decreases with increased dye concentration [7]. The explanation is supposed to be •OH radical generation is reduced at high dye concentrations on the catalyst surface because dye ions cover the active sites [45]. Another possible that numerous UVs may be absorbed by the dye molecules rather than the particles of TiO_2, which decreases the catalytic reaction efficiency as the concentrations of OH• and $O_2^{•-}$ decrease [6].

It is concluded that with an increasing initial dye concentration, the catalyst surface requirement for degradation also increases [7].

3.5.2. Effect of TiO_2 loading

The photocatalyst's contents and form are the most essential parameter affecting the photocatalytic degradation rate. A series of experiments were carried with various catalytic concentration ranges from 0.1 to 0.6 g L^{-1} at an optimal pH of 5.0 keeping the dye concentration of RhB and RRB at 6 and 25 mg L^{-1} respectively to determine the optimum catalyst concentration and their degradation plots are presented in Fig. 9. The degradation rate increased with increases in catalyst concentration because of the availability of active sites on the TiO_2 surface. The result is that the number of catalytic species increases the greater contents of hydroxyl radicals (•OH) and reactive oxygen species (ROS) was produced, which induces the electron–hole pair generation [46].

However, the reaction rate also decreases above a certain level of concentration and is independent of the concentration of the catalyst, with a negative effect; since the excess dosage of the catalytic particles shows screening effects that can prevent photons from reaching the inner catalyst surface [7].

According to the results of these experiments, the optimal reaction condition for RRB dye is 0.4 g L^{-1} catalyst contents for improved efficiency to 50% and 0.3 g L^{-1} TiO_2
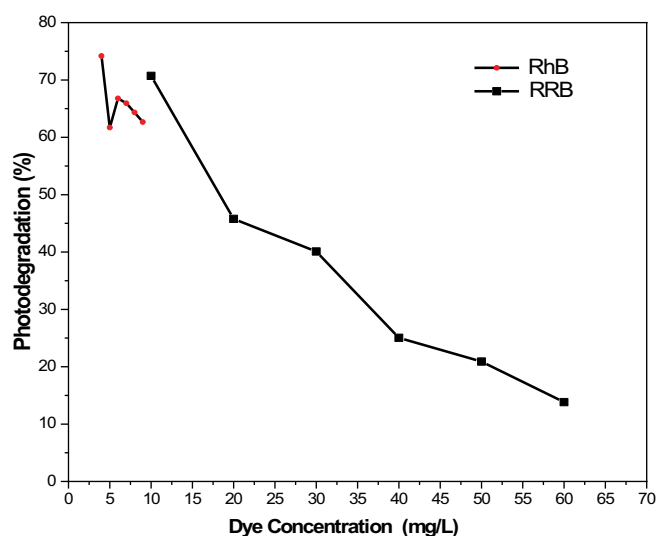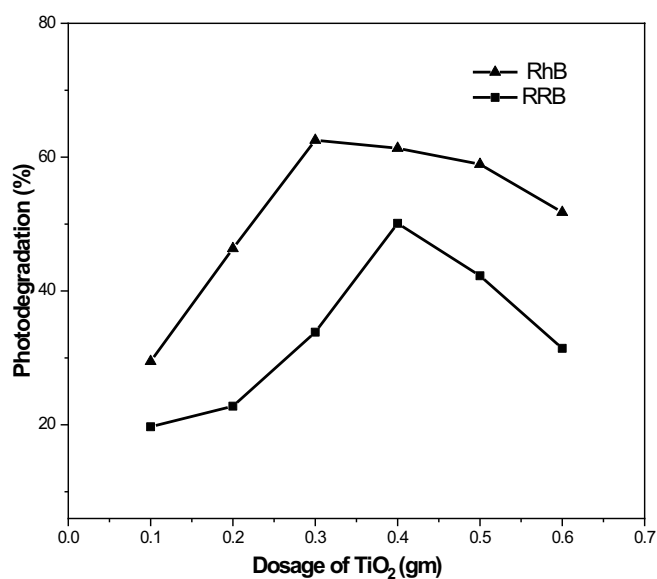

Fig. 9. Effect of TiO_2 contents prepared at 550°C on the photodegradation activity of RhB (6 mg L^{-1}) and RRB (25 mg L^{-1}) at 20 min irradiation time.
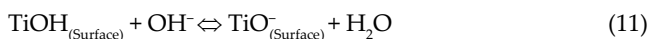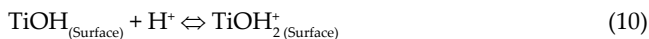
for RhB dye to increase performance by 63% as maximum degradation.

3.5.3. Effect of pH

The activity of the photocatalyst strongly artificial by the charging properties of the surface molecule, the organic molecule adsorption behavior on the photocatalyst surface, hydroxyl radical attack, and the reaction mechanism, which can further degrade the dye [7]. Thus, pH for determining photocatalytic removal efficiency is an important operational parameter.

The pH-effects understanding of the efficiency of the photodegradation process of dye is based on the surface ionization status as follows [7]:

$$TiOH_{(Surface)} + H^+ \Leftrightarrow TiOH_{2\,(Surface)}^+ \qquad (10)$$

$$TiOH_{(Surface)} + OH^- \Leftrightarrow TiO_{(Surface)}^- + H_2O \qquad (11)$$

The variations of pH between 2 and 10 for Rhodamine B and Remazol Red B dyes are shown in degradation curves (Fig. 10), for RhB (6 mg L^{-1}), RRB (25 mg L^{-1}) as initial concentration, and keeping TiO$_2$ dose for RhB and RRB dyes at 0.3 and 0.4 g L^{-1}, respectively under UV irradiation.

For TiO$_2$, the point of zero charge (pH$_{PZC}$) is 7.2. Therefore, the TiO$_2$ photocatalyst surface becomes positively charged in acidic media (pH < 7.2) converts under alkaline conditions (pH > 7.2) to negatively charged. Since the amphoteric activity of the semiconductor TiO$_2$, the photocatalytic process efficiencies highly depend on the reaction solution pH. At low pH, major oxidation species are the positive holes, which react to form hydroxyl radicals using hydroxide ions, the rate of dye adsorption on the TiO$_2$ particles strongly increased because of the electrostatic attraction of the positively charged TiO$_2$ with the dye. Also, the molecular structure of the dye may, in acidic conditions, change to an unstable quinoid structure that can be easily destroyed. Thus, Improve the efficiency of processes [47].

At increasing pH, a columbic repulsion occurs between the negatively charged TiO$_2$ and the $^-$OH species that prevents OH$^•$ ion radical formation, which at a higher pH value is unstable and reduces photocatalytic degradation [48]. The adsorption and redox activities may change the characteristics of protonation or deprotonation as another explanation [7].

In acidic conditions, this experiment maximizes anionic dyes' photocatalytic activity, followed by a decrease in the basic medium [49]. For both RhB and RRB dyes, the efficiency of degradation was higher in pH 5.

3.6. Degradation kinetics

The photocatalytic activity of a prepared TiO$_2$ sample under simulated UV radiation is estimated by Rhodamine B (RhB) and Remazol Red B (RRB) as model dyes. The first-order reaction shown in Eq. (2), can explain the photodegradation kinetics of RhB and RRB on the photocatalyst surface. The linear relationship between $\ln(C_0/C_t)$ and irradiation time (t) for the RhB and RRB solution is described in Fig. 11. For the analyzed TiO$_2$ photocatalyst, the rate constants were calculated from the slope of the linear fitting line as shown in Fig. 11. A good correlation was observed, with the first-order reaction kinetics ($R^2_{RhB} = 0.99632$) ($R^2_{RRB} = 0.99565$). In our case, because RhB has lower bond dissociation energy, RhB degraded faster than RRB. The mechanism of degradation involves breaking old bonds and forming up new ones. The theory of energy bond dissociation states that chemical bonds with lower bond dissociation energy are more easily broken and form new bonds conveniently [50,51]. The RhB and RRB rate constant was respectively 0.0557 and 0.0455 min^{-1}.
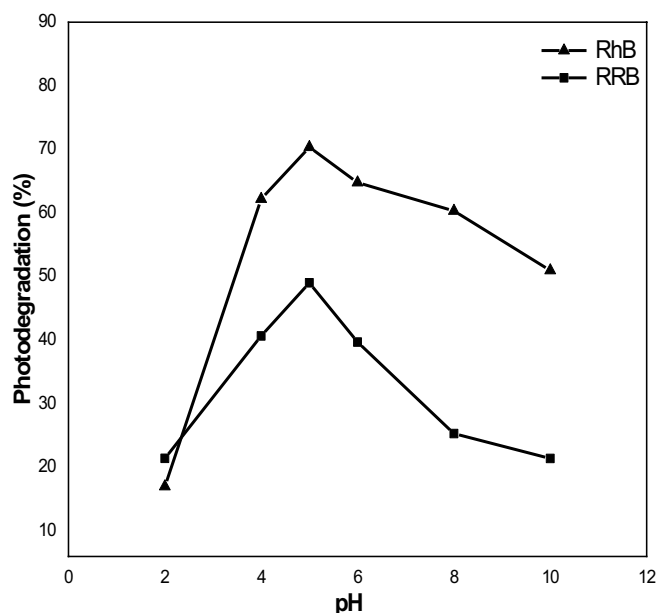

Fig. 10. Effect of pH on the properties of TiO$_2$ at 550°C (20 min irradiation time, 6 mg L^{-1} for RRB and 25 mg L^{-1} for RRB initial dye concentration, and the dose of TiO$_2$ for RhB (0.3 g L^{-1}) and RRB (0.4 g L^{-1})).

3.7. TiO$_2$ photocatalyst stability

Besides the photocatalytic properties, the stability of photocatalysis is significant in large-scale processes. Thus, TiO$_2$ recycling experiments were performed for the stability of TiO$_2$ photocatalyst on RhB and RRB photocatalytic degradations under UV irradiation. After each cycle, the photocatalyst was collected with a centrifuge, then washed using distilled water and ethanol, and dehydrated in an oven at 100°C. Then a further degradation of the sample was reused. As seen, after three cycles the efficiency of RhB and RRB degradation has dropped from 93.8 to 87 and 90.7 to 85, respectively. The photocatalyst deactivation because of the unavoidable loss of photocatalyst during the cycle processes and probably associated with some surface poisoning, which can be caused by intermediate adsorption. Dutta and Ray [52] experimental results suggest that highly adsorbed intermediates occupied active sites on the catalyst surface and caused a modest reduction in photocatalytic activity. Therefore, the TiO$_2$ photocatalyst remains high photocatalytic activity and stability under UV irradiation for a long time and presenting a slight loss in its degradation efficiency.

3.8. Mechanism of photodegradation

The photocatalytic reaction contains photoexcitation, charge separation and migration, and surface oxidation-reduction reactions [53]. The reactive species generated during illumination of photocatalyst are h$^+$, $^-$OH, and O$_2^{•-}$. To understand the mechanism of TiO$_2$ for the degradation of RhB and RRB dye, it is necessary to identify which reactive species plays a major role in the photocatalytic degradation process. During the
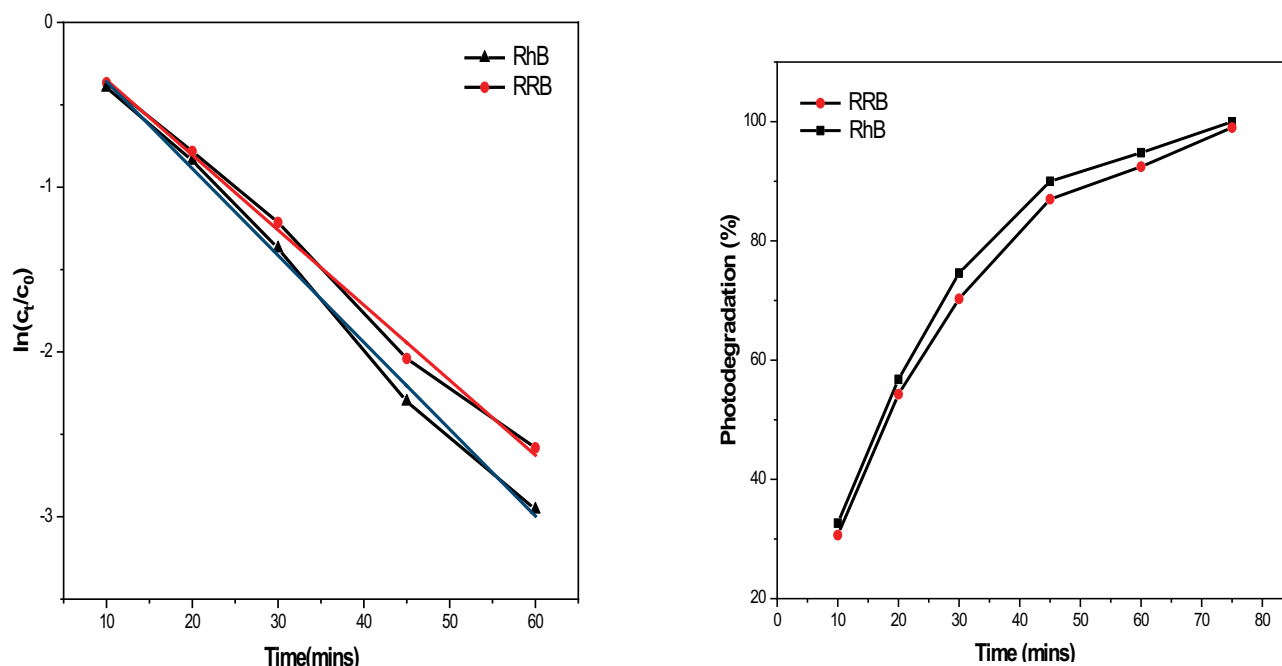
Fig. 11. The photocatalytic degradation efficiency of RhB and RRB using TiO_2 under simulated UV irradiation.
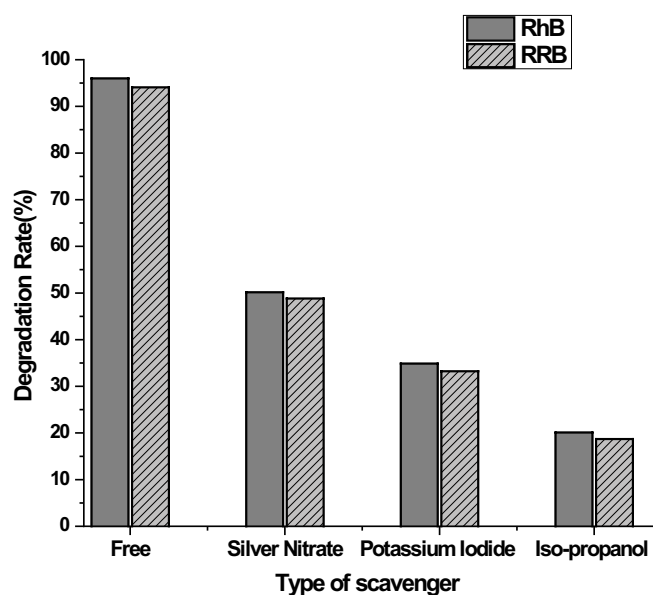

Fig. 12. Photodegradation ratio of RhB and RRB over TiO_2 in the absence and presence of various scavengers (silver nitrate, potassium iodide, and isopropanol) under UV irradiation, initial dye concentration of RhB (6 mg L^{-1}) and RRB (25 mg L^{-1}) solution, the dose of TiO_2 for RhB (0.3 g L^{-1}) and RRB (0.4 g L^{-1}) and pH = 5.

photodegradation of dyes over TiO_2, the e^-, h^+, $OH^\bullet$ and $O_2^{\bullet-}$ are reduced by adding silver nitrate (e^- scavenger), potassium iodide (h^+ scavenger), and isopropanol ($OH^\bullet$ scavenger), into the reaction solution, respectively [54]. Fig. 12 shows the degradation rate in the presence and absence of the scavengers. The addition of silver nitrate

showed a slight difference in the photocatalytic degradation of RhB and RRB dye. However, the photodegradation percentage of RhB and RRB are considerably reduced with the addition of a scavenger for isopropanol, potassium iodide [55]. Hence, the active species responsible for photocatalytic degradation of RhB and RRB is the hydroxyl radicals ($OH^\bullet$) and the efficiency of photocatalyst for degradation of the two dyes is mainly influenced by the concentration of the generated $OH^\bullet$ radicals.

Photo-generated catalysis is also called "a sensitized photoreaction". The photocatalyst is a semiconductor that can act as a sensitizer for light-reduced redox processes because of their electronic structure, which is characterized by a filled valence band and an empty conduction band. The mechanism of the process has been discussed in the literature [56–59].

When a photon with an energy of $h\nu$ matches or exceeds the bandgap energy, for example, of the semiconductor, an electron, $e_{(CB)}^-$, is promoted from the valence band, VB, into the conduction band, CB, leaving a hole, $(h_{(VB)}^+)$.

Photoexcitation: $TiO_2 + h\nu \rightarrow TiO_2 (h_{(VB)}^+) + TiO_2 (e_{(CB)}^-)$ (12)
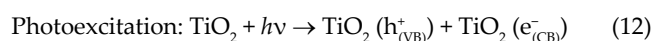
Excited-state conduction band electrons and valence band holes can recombine and dissipate the input energy as heat.

Recombination pathway: $TiO_2 (h_{(VB)}^+) + TiO_2 (e_{(CB)}^-) \rightarrow TiO_2 + heat$ (13)
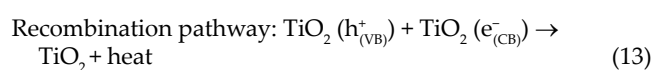
while the holes will interact with the surrounding water to produce hydroxyl radicals ($OH^\bullet$).

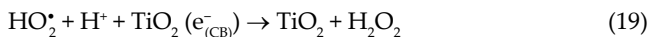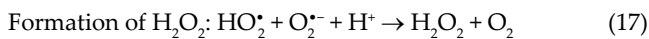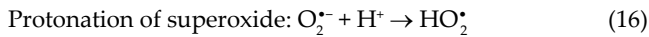Ionization of water: $H_2O + TiO_2 (h_{(VB)}^+) \rightarrow TiO_2 + OH^\bullet + H^+$ (14)
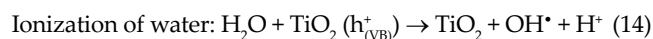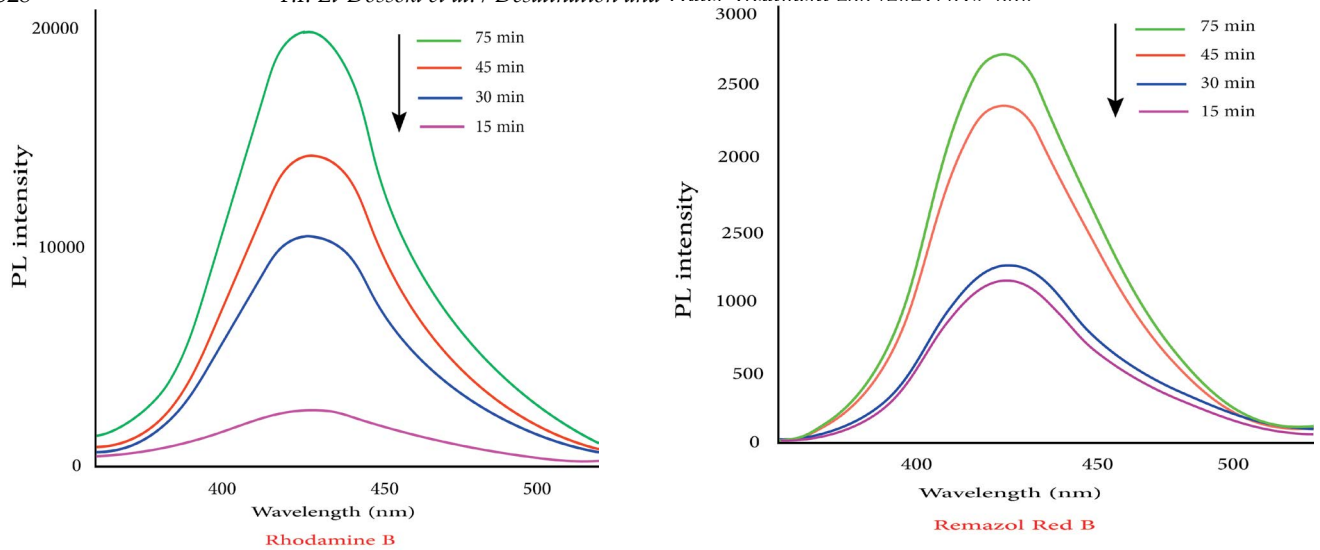
Fig. 13. Photoluminescence spectra of TiO_2 + TPA after irradiation (initial dye concentration of RhB (6 mg L^{-1}) and RRB (25 mg L^{-1}) solution, dose of TiO_2 for RhB (0.3 g L^{-1}) and RRB (0.4 g L^{-1}), 5×10^{-5} M terephthalic acid, and pH = 5) with the excitation wavelength of 315 nm.
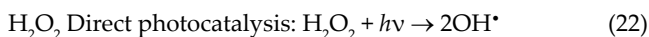
The electrons will interact with the surrounding oxygen and produce superoxide radicals ($O_2^{•-}$),

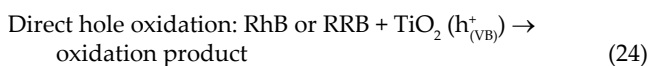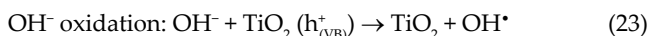Oxygen ionosorption: TiO_2 ($e_{(CB)}^-$) + O_2 → TiO_2 + $O_2^{•-}$ (15)
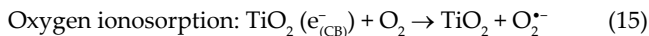
The superoxide ($O_2^{•-}$) produced gets protonated forming hydroperoxyl radical ($HO_2^•$) and then formation H_2O_2 (Reactions (16)–(19)).

Protonation of superoxide: $O_2^{•-}$ + H^+ → $HO_2^•$ (16)

Formation of H_2O_2: $HO_2^•$ + $O_2^{•-}$ + H^+ → H_2O_2 + O_2 (17)

$2\,HO_2^•$ → H_2O_2 + O_2 (18)

$HO_2^•$ + H^+ + TiO_2 ($e_{(CB)}^-$) → TiO_2 + H_2O_2 (19)

During the reaction, H_2O_2 can produce highly reactive hydroxyl by reacting with $O_2^{•-}$ (Reaction (20)) or with ($e_{(CB)}^-$) (Reaction (21)) or by direct photolysis (Reaction (22)).

H_2O_2 + $O_2^{•-}$ → $OH^•$ + OH^- + O_2 (20)

H_2O_2 + TiO_2 ($e_{(CB)}^-$) → TiO_2 + $OH^•$ + OH^- (21)

H_2O_2 Direct photocatalysis: H_2O_2 + $h\nu$ → $2OH^•$ (22)
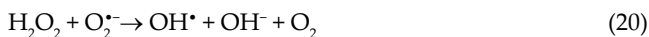
The ($h_{(VB)}^+$) is a strong oxidant, which reacts with electron donors like hydroxide ions to form hydroxyl radicals (Reactions (23)) and reacts with pollutant such as dye (Reaction (24)).

OH^- oxidation: OH^- + TiO_2 ($h_{(VB)}^+$) → TiO_2 + $OH^•$ (23)

Direct hole oxidation: RhB or RRB + TiO_2 ($h_{(VB)}^+$) → oxidation product   (24)

Hydroxyl radicals react with organic pollutants and lead to the total mineralization of most of them into water (H_2O) and carbon dioxide (CO_2).

Direct photodegradation by $OH^•$: RhB or RRB + $OH^•$ → products (CO_2 and H_2O)   (25)
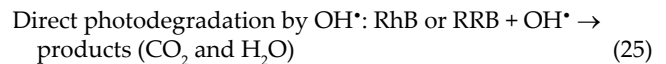
while the photo-generated electrons ($e_{(CB)}^-$) is a potential redactor which could either reduce the dye directly.

Direct electron reduction: RhB or RRB + TiO_2 ($e_{(CB)}^-$) → reduction product   (26)
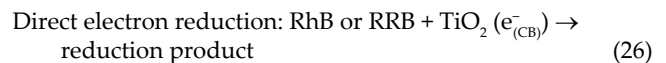
The formation of $OH^•$ free radicals is determined using photoluminescence studies using terephthalic acid (TPA) as a probe molecule. TPA reacts with $^•OH$ free radicals to yield 2-hydroxyterphthalic acid, which shows a characteristic luminescence peak at 420 nm [60]. The intense luminescence peak at 430 nm for the sample containing TiO_2 + TPA after irradiation for 15, 30, 45, and 75 min showed clearly the presence of $^•OH$ free radicals during irradiation (Fig. 13).

4. Conclusions

This study investigated the photocatalytic activity of TiO_2 as a photocatalyst to treat RhB and RRB dyes in aqueous solutions under irradiation of ultraviolet light. A single step sol–gel method synthesized the TiO_2 sample, and various techniques of spectroscopy were characterized for the sample. The TiO_2 was present in a hexagonal wurtzite phase based on the measurement of the XRD and SEM, and the TiO_2 size was 13.1 am at 550°C. The highest photocatalytic removal of RhB and RRB from aqueous solution was achieved by using TiO_2 as a photocatalyst, confirmed also by the evaluation of the kinetic constant for RhB and RRB degradation. The effect of pH, catalyst dose

and initial dye concentration as operating parameters was estimated. The degradation of RhB and RRB was observed to fit the kinetics of the first-order, and the main species were OH• radicals. During irradiation, the OH• free radicals' formation was ascertained using terephthalic acid as a molecular probe by photoluminescence experiments.

References

[1] N. Hassan, A. Shahat, A. El-Didamony, M.G. El-Desouky, A.A. El-Bindary, Synthesis and characterization of ZnO nanoparticles via zeolitic imidazolate framework-8 and its application for removal of dyes, J. Mol. Struct., 1210 (2020) 128029, doi: 10.1016/j.molstruc.2020.128029.

[2] H. An, Y. Qian, X. Gu, W.Z. Tang, Biological treatment of dye wastewaters using an anaerobic-oxic system, Chemosphere, 33 (1996) 2533–2542.

[3] R. Anliker, Ecotoxicology of dyestuffs—a joint effort by industry, Ecotoxicol. Environ. Saf., 3 (1979) 59–74.

[4] M.A. Brown, S.C. De Vito, Predicting azo dye toxicity, Crit. Rev. Env. Sci. Technol., 23 (1993) 249–324.

[5] K.S. Abou-Melha, G.A.A. Al-Hazmi, I. Althagafi, R. Shah, F. Shaaban, N.M. El-Metwaly, A.A. El-Bindary, Preparation of CuO nanoparticles via organometallic chelate for the removal of acid red 57 from aqueous solutions, Desal. Water Treat., 222 (2021) 282–294.

[6] M. Hao, M. Qiu, H. Yang, B. Hu, X. Wang, Recent advances on preparation and environmental applications of MOF-derived carbons in catalysis, Sci. Total Environ., 760 (2021) 143333, doi: 10.1016/j.scitotenv.2020.143333.

[7] I.K. Konstantinou, T.A. Albanis, TiO₂-assisted photocatalytic degradation of azo dyes in aqueous solution: kinetic and mechanistic investigations: a review, Appl. Catal., B, 49 (2004) 1–14.

[8] X. Liu, H. Pang, X. Liu, Q. Li, N. Zhang, L. Mao, M. Qiu, B. Hu, H. Yang, X. Wang, Orderly porous covalent organic frameworks-based materials: superior adsorbents for pollutants removal from aqueous solutions, Innovation, 2 (2021) 100076, doi: 10.1016/j.xinn.2021.100076.

[9] R.W. Matthews, Photooxidative degradation of coloured organics in water using supported catalysts. TiO₂ on sand, Water Res., 25 (1991) 1169–1176.

[10] A.K. Ray, A.A.C.M. Beenackers, Development of a new photocatalytic reactor for water purification, Catal. Today, 40 (1998) 73–83.

[11] K. Tanaka, K. Padermpole, T. Hisanaga, Photocatalytic degradation of commercial azo dyes, Water Res., 34 (2000) 327–333.

[12] H.A. Kiwaan, F.S. Mohamed, N.A. El-Ghamaz, N.M. Beshry, A.A. El-Bindary, Experimental and electrical studies of Na-X zeolite for the adsorption of different dyes, J. Mol. Liq., 332 (2021) 115877, doi: 10.1016/j.molliq.2021.115877.

[13] C. Tang, V. Chen, The photocatalytic degradation of reactive black 5 using TiO₂/UV in an annular photoreactor, Water Res., 38 (2004) 2775–2781.

[14] A.Z. El-Sonbati, I.M. El-Deen, M.A. El-Bindary, Adsorption of hazardous azorhodanine dye from an aqueous solution using rice straw fly ash, J. Dispersion Sci. Technol., 37 (2016) 715–722.

[15] E. Bizani, K. Fytianos, I. Poulios, V. Tsiridis, Photocatalytic decolorization and degradation of dye solutions and wastewaters in the presence of titanium dioxide, J. Hazard. Mater., 136 (2006) 85–94.

[16] N. Daneshvar, D. Salari, A.R. Khataee, Photocatalytic degradation of azo dye acid red 14 in water: investigation of the effect of operational parameters, J. Photochem. Photobiol., A, 157 (2003) 111–116.

[17] S. Ledakowicz, M. Gonera, Optimisation of oxidants dose for combined chemical and biological treatment of textile wastewater, Water Res., 33 (1999) 2511–2516.

[18] A. Houas, H. Lachheb, M. Ksibi, E. Elaloui, C. Guillard, J.-M. Herrmann, Photocatalytic degradation pathway of methylene blue in water, Appl. Catal., B, 31 (2001) 145–157.

[19] L. Yao, H. Yang, Z. Chen, M. Qiu, B. Hu, X. Wang, Bismuth oxychloride-based materials for the removal of organic pollutants in wastewater, Chemosphere, 273 (2021) 128576, doi: 10.1016/j.chemosphere.2020.128576.

[20] O. Carp, C.L. Huisman, A. Reller, Photoinduced reactivity of titanium dioxide, Prog. Solid State Chem., 32 (2004) 33–177.

[21] J. Grzechulska, A.W. Morawski, Photocatalytic decomposition of azo-dye acid black 1 in water over modified titanium dioxide, Appl. Catal., B, 36 (2002) 45–51.

[22] S.P. Patil, V.S. Shrivastava, G.H. Sonawane, S.H. Sonawane, Synthesis of novel Bi₂O₃–montmorillonite nanocomposite with enhanced photocatalytic performance in dye degradation, J. Environ. Chem. Eng., 3 (2015) 2597–2603.

[23] Nasikhudin, M. Diantoro, A. Kusumaatmaja, K. Triyana, Study on photocatalytic properties of TiO₂ nanoparticle in various pH condition, J. Phys. Conf. Ser., 1011 (2018) 012069.

[24] J.P. Lorimer, T.J. Mason, M. Plattes, S.S. Phull, D.J. Walton, Degradation of dye effluent, Pure Appl. Chem., 73 (2001) 1957–1968.

[25] R. Jain, M. Mathur, S. Sikarwar, A. Mittal, Removal of the hazardous dye Rhodamine B through photocatalytic and adsorption treatments, J. Environ. Manage., 85 (2007) 956–964.

[26] S.M.I. Morsy, S.A. Shaban, A.M. Ibrahim, M.M. Selim, Characterization of cobalt oxide nanocatalysts prepared by microemulsion with different surfactants, reduction by hydrazine and mechanochemical method, J. Alloys Compd., 486 (2009) 83–87.

[27] S.Y. Lee, D. Kang, S. Jeong, H.T. Do, J.H. Kim, Photocatalytic degradation of rhodamine B dye by TiO2 and gold nanoparticles supported on a floating porous polydimethylsiloxane sponge under ultraviolet and visible light irradiation, ACS Omega, 5 (2020) 4233–4241.

[28] H.A. Kiwaan, T.M. Atwee, E.A. Azab, A.A. El-Bindary, Efficient photocatalytic degradation of Acid Red 57 using synthesized ZnO nanowires, J. Chin. Chem. Soc., 66 (2019) 89–98.

[29] S. Brunauer, P.H. Emmett, E. Teller, Adsorption of gases in multimolecular layers, J. Am. Chem. Soc., 60 (1938) 309–319.

[30] Q. Zhang, M. Xu, M. You, Q. Zhang, H. Yuan, K. Ostrikov, Oxygen vacancy-mediated ZnO nanoparticle photocatalyst for degradation of methylene blue, Appl. Sci., 8 (2018) 353, doi: 10.3390/app8030353.

[31] A. Jain, D. Vaya, Photocatalytic activity of TiO₂ nanomaterial, J. Chil. Chem. Soc., 62 (2017) 3683–3690.

[32] K. Fischer, P. Schulz, I. Atanasov, A. Abdul Latif, I. Thomas, M. Kühnert, A. Prager, J. Griebel, A. Schulze, Synthesis of high crystalline TiO₂ nanoparticles on a polymer membrane to degrade pollutants from water, Catalysts, 8 (2018) 376, doi: 10.3390/catal8090376.

[33] L. Yang, S. Luo, Y. Li, Y. Xiao, Q. Kang, Q. Cai, High efficient photocatalytic degradation of p-nitrophenol on a unique Cu₂O/TiO₂ p-n heterojunction network catalyst, Environ. Sci. Technol., 44 (2010) 7641–7646.

[34] A.L. Patterson, The Scherrer formula for X-ray particle size determination, Phys. Rev., 56 (1939) 978–982.

[35] A.K. Tripathi, M.K. Singh, M.C. Mathpal, S.K. Mishra, A. Agarwal, Study of structural transformation in TiO₂ nanoparticles and its optical properties, J. Alloys Compd., 549 (2013) 114–120.

[36] P. Reeves, R. Ohlhausen, D. Sloan, K. Pamplin, T. Scoggins, C. Clark, B. Hutchinson, D. Green, Photocatalytic destruction of organic dyes in aqueous TiO₂ suspensions using concentrated simulated and natural solar energy, Sol. Energy, 48 (1992) 413–420.

[37] O.R. Fonseca-Cervantes, A. Pérez-Larios, V.H. Romero Arellano, B. Sulbaran-Rangel, C.A. Guzmán González, Effects in band gap for photocatalysis in TiO₂ support by adding gold and ruthenium, Processes, 8 (2020) 1032, doi: 10.3390/pr8091032.

[38] S. Singh, S. Kumar, Investigation of optical constants and optical band gap for amorphous Se₄₀₋ₓTe₆₀Agₓ thin films, Chalcogenide Lett., 14 (2017) 139–146.

[39] H.A. Kiwaan, T.M. Atwee, E.A. Azab, A.A. El-Bindary, Photocatalytic degradation of organic dyes in the presence of nanostructured titanium dioxide, J. Mol. Struct., 1200 (2020) 127115, doi: 10.1016/j.molstruc.2019.127115.

[40] G. Li, B.-D. Wang, Q. Sun, W.-Q. Xu, Y.-F. Han, Visible-light photocatalytic activity of Fe and/or Ni doped ilmenite derived-titanium dioxide nanoparticles, J. Nanosci. Nanotechnol., 19 (2019) 3343–3355.

[41] A.A. El-Bindary, S.M. El-Marsafy, A.A. El-Maddah, Enhancement of the photocatalytic activity of ZnO nanoparticles by silver doping for the degradation of AY99 contaminants, J. Mol. Struct., 1191 (2019) 76–84.

[42] E.E. El-Katori, M.A. Ahmed, A.A. El-Bindary, A.M. Oraby, Impact of CdS/SnO$_2$ heterostructured nanoparticle as visible light active photocatalyst for the removal methylene blue dye, J. Photochem. Photobiol., A, 392 (2020) 112403, doi: 10.1016/j.jphotochem.2020.112403.

[43] M.M. Haque, M. Muneer, TiO$_2$-mediated photocatalytic degradation of a textile dye derivative, bromothymol blue, in aqueous suspensions, Dyes Pigm., 75 (2007) 443–448.

[44] M. Zarei, D. Salari, A. Niaei, A. Khataee, Peroxi-coagulation degradation of C.I. Basic Yellow 2 based on carbon-PTFE and carbon nanotube-PTFE electrodes as cathode, Electrochim. Acta, 54 (2009) 6651–6660.

[45] G. Tafurt-García, L. Copete-Pertuz, M.S. Pérez-Grisales, A.L. Mora-Martínez, G. Correa Londoño, M. Castrillón-Tobón, Decolorization of Reactive Black 5 dye by heterogeneous photocatalysis with TiO$_2$/UV, Rev. Colomb. Química, 47 (2018) 36–44.

[46] K.M. Reza, A. Kurny, F. Gulshan, Parameters affecting the photocatalytic degradation of dyes using TiO$_2$: a review, Appl. Water Sci., 7 (2017) 1569–1578.

[47] S. Chitra, K. Paramasivan, P.K. Sinha, K.B. Lal, Ultrasonic treatment of liquid waste containing EDTA, J. Cleaner Prod., 12 (2004) 429–435.

[48] X. Liu, R. Ma, L. Zhuang, B. Hu, J. Chen, X. Liu, X. Wang, Recent developments of doped g-C$_3$N$_4$ photocatalysts for the degradation of organic pollutants, Crit. Rev. Env. Sci. Technol., 51 (2021) 751–790.

[49] M.F. Abid, A.A. Abdulrahman, N.H. Hamza, Hydrodynamic and kinetic study of a hybrid detoxification process with zero liquid discharge system in an industrial wastewater treatment, J. Environ. Health Sci. Eng., 12 (2014) 145, doi: 10.1186/s40201-014-0145-z.

[50] R. Singh, S. Dutta, Synthesis and characterization of solar photoactive TiO$_2$ nanoparticles with enhanced structural and optical properties, Adv. Powder Technol., 29 (2018) 211–219.

[51] L. Wu, Q. Xie, Y. Lv, Z. Zhang, Z. Wu, X. Liang, M. Lu, Y. Nie, Degradation of methylene blue by dielectric barrier discharge plasma coupled with activated carbon supported on polyurethane foam, RSC Adv., 9 (2019) 25967–25975.

[52] P.K. Dutta, A.K. Ray, Experimental investigation of Taylor vortex photocatalytic reactor for water purification, Chem. Eng. Sci., 59 (2004) 5249–5259.

[53] A.R. Khataee, M.B. Kasiri, Photocatalytic degradation of organic dyes in the presence of nanostructured titanium dioxide: influence of the chemical structure of dyes, J. Mol. Catal. A: Chem., 328 (2010) 8–26.

[54] B.A. van Driel, P.J. Kooyman, K.J. van den Berg, A. Schmidt-Ott, J. Dik, A quick assessment of the photocatalytic activity of TiO$_2$ pigments — from lab to conservation studio!, Microchem. J., 126 (2016) 162–171.

[55] Y. Nam, J.H. Lim, K.C. Ko, J.Y. Lee, Photocatalytic activity of TiO$_2$ nanoparticles: a theoretical aspect, J. Mater. Chem. A, 7 (2019) 13833–13859.

[56] A.B. Prevot, C. Baiocchi, M.C. Brussino, E. Pramauro, P. Savarino, V. Augugliaro, G. Marcì, L. Palmisano, Photocatalytic degradation of acid blue 80 in aqueous solutions containing TiO$_2$ suspensions, Environ. Sci. Technol., 35 (2001) 971–976.

[57] C. Galindo, P. Jacques, A. Kalt, Photodegradation of the aminoazobenzene acid orange 52 by three advanced oxidation processes: UV/H$_2$O$_2$, UV/TiO$_2$ and VIS/TiO$_2$: comparative mechanistic and kinetic investigations, J. Photochem. Photobiol., A, 130 (2000) 35–47.

[58] N. Guettaï, H. Ait Amar, Photocatalytic oxidation of methyl orange in presence of titanium dioxide in aqueous suspension. Part I: Parametric study, Desalination, 185 (2005) 427–437.

[59] H.A. Kiwaan, F.Sh. Mohamed, N.A. El-Ghamaz, N.M. Beshry, A.A. El-Bindary, Experimental and electrical studies of zeolitic imidazolate framework-8 for the adsorption of different dyes, J. Mol. Liq., 338 (2021) 116670, doi: 10.1016/j.molliq.2021.116670.

[60] X.H. Lin, S.N. Lee, W. Zhang, S.F.Y. Li, Photocatalytic degradation of terephthalic acid on sulfated titania particles and identification of fluorescent intermediates, J. Hazard. Mater., 303 (2016) 64–75.